The Astrophysical Journal, 657:790–804, 2007 March 10

A NEAR-INFRARED STUDY OF 2MASS BARS IN LOCAL GALAXIES: AN ANCHOR FOR HIGH-REDSHIFT STUDIES

Karín Menéndez-Delmestre,[1] Kartik Sheth,[1,2] Eva Schinnerer,[3] Thomas H. Jarrett,[4] and Nick Z. Scoville[1]

Received 2006 April 14; accepted 2006 November 14

ABSTRACT

We have measured the fraction of bars in nearby spiral galaxies using near-infrared J, H, and K_s images of 151 spiral galaxies from 2MASS. This local sample provides an anchor for the study of the evolution of the bar fraction and bar properties with redshift. We identify bars by analyzing the full two-dimensional light distribution and requiring a combined ellipticity and position angle signature. The combined "bar signature" is found in 59% of the galaxies. The bar fraction increases to 67% when we include "candidate" bars, where only the ellipticity signature is present. We also measure the change in the bar fraction as a function of bar size; the bar fraction drops to 31% for bars with a semimajor axis larger than 4 kpc. We find that infrared bars typically extend to one-third of the galactic disk, with a deprojected relative size of $\langle a_{\rm bar}/R_{25}\rangle \sim 0.3 \pm 0.2$. Early-type spirals host significantly larger bars, consistent with earlier studies. The $\langle a_{\rm bar}/R_{25}\rangle$ is 2 times larger in early types than in late types. The typical bar axial ratio (b/a) is $\sim$0.5, with a weak trend of higher axial ratios for larger bars.

Subject headings: galaxies: spiral — galaxies: structure — infrared: galaxies — methods: data analysis — techniques: photometric

Online material: machine-readable tables

1. INTRODUCTION

Bars play a central role in the evolution of galaxies. The nonaxisymmetry of the bar induces large-scale streaming motions in the stars and the gas (Athanassoula 1992a; Piner et al. 1995; Teuben 1995). Unlike stars, the gas is collisional and dissipative, losing angular momentum and flowing inward down the bar dust lanes (Combes & Gerin 1985; Athanassoula 1992b; Regan et al. 1997, 1999; Sheth et al. 2000, 2002, 2005). This inflow leads to dramatic changes in the host galaxy such as accumulation of molecular gas in the central kiloparsec (Sakamoto et al. 1999; Sheth et al. 2005), smoothing of the chemical abundance gradient (Martin & Roy 1994), inducement of circumnuclear star formation (see Ho et al. 1997a, 1997b and references therein) and (possibly) the formation of bulges and pseudobulges (Norman et al. 1996; Kormendy & Kennicutt 2004; Sheth et al. 2005), fueling of active galactic nuclei (Shlosman et al. 1989), and perhaps the destruction of the bar itself (Norman et al. 1996; Das et al. 2003). Understanding the bar fraction and bar properties is therefore critical to understanding the evolution of spiral galaxies.

As early as 1963, using photographic plates that are sensitive to blue light, de Vaucouleurs (1963) found that 35% of all nearby spiral galaxies (S0/a–Sd) are strongly barred (SB). An additional 29% were classified as "intermediately" barred (SAB) spirals. With the advent of near-infared (NIR) detectors, previously undiscovered bars were seen at infrared wavelengths (e.g., Hackwell & Schweizer 1983; Scoville et al. 1988; Thronson et al. 1989; Mulchaey & Regan 1997; Seigar & James 1998; Jarrett et al. 2003); these were typically small nuclear bars at the centers of nearby spirals, where dust obscuration can be high and variable. In hindsight these discoveries are not surprising since bars are stellar structures that are best seen at longer wavelengths, where the veiling effects of dust extinction and star formation are minimized compared to optical wavelengths. The NIR light is dominated by old stars which constitute the bulk of the stellar mass; the NIR, therefore, is a more reliable tracer of a galaxy's gravitational potential than optical light. Although large format NIR cameras have become more common over the last decade, there are only a few large and homogeneous NIR surveys of nearby spirals, and of these, only the Ohio State University Bright Spiral Galaxy Survey (OSUBSGS; Eskridge et al. 2002), with 205 spirals with $T \geq 0$, $B \leq 12$, and $D \leq 6'$ has been used to examine the fraction of bars in the H band (Eskridge et al. 2000; Whyte et al. 2002; Laurikainen et al. 2004 [hereafter E2000, W2002 and L2004, respectively]; Marinova & Jogee 2007). Several other studies have examined the bar fraction in the optical and NIR between active and nonactive galaxies, to determine the role of bars in feeding active galactic nuclei (AGNs) (Mulchaey & Regan 1997; Knapen et al. 2000; Laine et al. 2002; Laurikainen et al. 2004).

The advent of large, deep extragalactic surveys such as COSMOS, GOODS, and GEMS (Scoville et al. 2007; Dickinson et al. 2003; Rix et al. 2004) has triggered studies that explore the evolution of the bar fraction with redshift (Sheth et al. 2003, 2004; Elmegreen et al. 2004; Jogee et al. 2004). A prerequisite for evaluating the results of these high-redshift studies is a well-determined bar fraction in the local universe.

Using H-band imaging of 186 and 113 nearby galaxies respectively, E2000 and W2002 classified $\sim\frac{3}{4}$ of the spirals as barred. E2000 relied on visual inspection to identify bars, like earlier optical studies (e.g., Third Reference Catalog of Bright Galaxies [de Vaucouleurs et al. 1991, hereafter RC3]), while W2002 relied on an automated method of measuring a bar based on the difference in the axial ratio and position angles of a best-fit ellipse to one interior and one exterior isophote; this method is a refinement of the bar identification method used by Abraham et al. (1996).

Although the eye is an excellent classification tool, visual inspection of images is unreliable for poor-quality and low signal-to-noise (S/N) data. Especially in the context of high-redshift galaxies, visual classification quickly becomes difficult in view

[1] California Institute of Technology, Department of Astronomy, Pasadena, CA.
[2] *Spitzer* Science Center, California Institute of Technology, Pasadena, CA.
[3] Max-Planck-Institute for Astronomy, Heidelberg, Germany.
[4] Infrared Processing and Analysis Center, California Institute of Technology, Pasadena, CA.

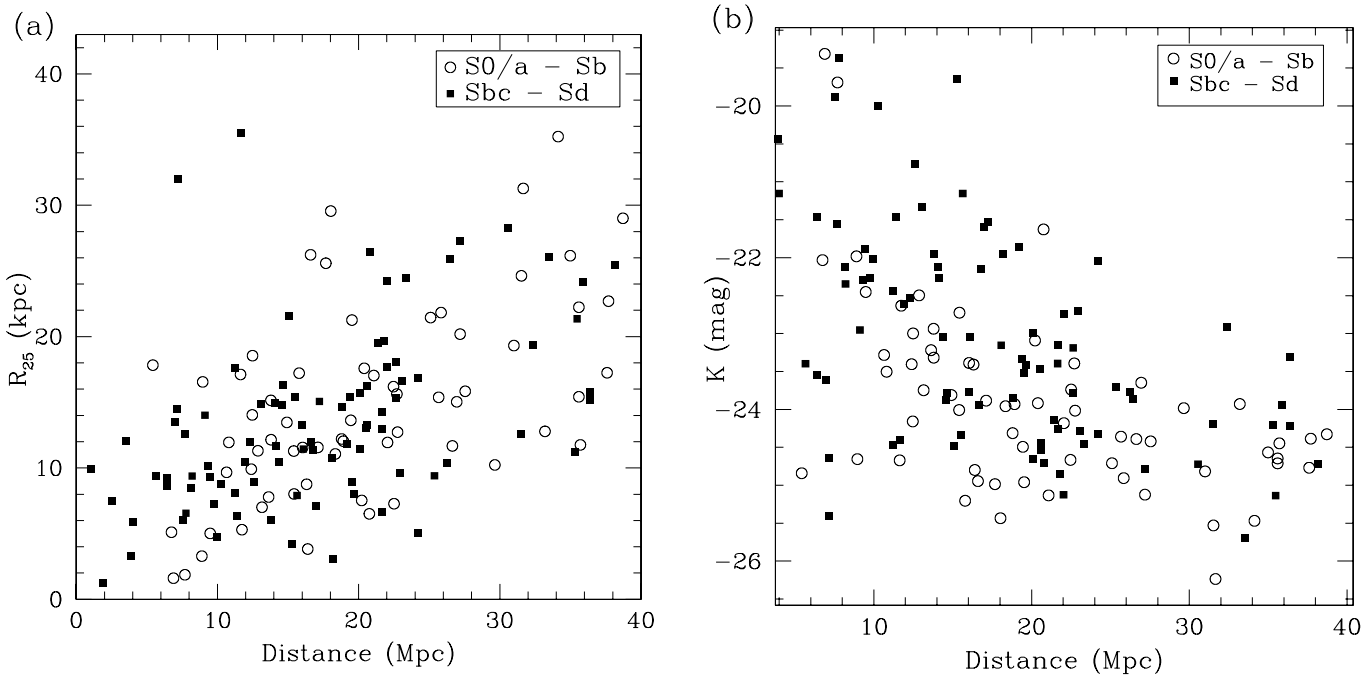

FIG. 1.—(*a*) Galaxy optical radius as a function of distance for our 2MASS spiral sample. (*b*) Same plot for absolute *K*-band magnitude. Early-type (S0/a–Sb) and late-type (Sbc–Sd) spirals are shown as open circles and filled squares, respectively.

of the significant decline in the spatial resolution (e.g., Fig. 3 of Sheth et al. 2003) or decreased S/N (due to the cosmological surface brightness dimming) with increasing redshift. Classification by eye is also tedious for large data sets and is subjective when comparing data sets of varying quality. In such cases an automated method for bar identification is more useful as it has the advantage of reproducibility and can be applied to large data sets. Moreover, an automated algorithm that uses the full two-dimensional light distribution is likely more robust than one that relies on a small number of isophotes.

An accurate measurement of the bar fraction also depends on a variety of selection biases such as surface brightness limits, S/N, inclination, and spatial resolution (Sheth et al. 2003, 2004). The measurement of the bar fraction is particularly sensitive to the spatial resolution of the data. Sheth et al. (2003) show how the bar fraction measured in the Hubble Deep Field–North using the coarse NICMOS data is comparable to the local RC3 fraction when the bar size is taken into account. It is, therefore, critical to have accurate measurement of the bar size distribution.

A number of studies have looked at the bar size distribution of optically selected (i.e., RC3 SB/SAB) local bars (Kormendy 1979; Elmegreen & Elmegreen 1985; Martin 1995; Erwin 2005). These optical studies have found that bars in early-type spirals tend to be longer than those found in late types. Laine et al. (2002) and L2004 have compared properties of *H*-band–selected bars in active and nonactive galaxies.

In this paper we present a detailed NIR morphological analysis of the local spiral population imaged by the Two Micron All Sky Survey (Skrutskie et al. 2006) Large Galaxy Atlas (hereafter, 2MASS LGA; Jarrett et al. 2003). We identify bars and characterize their sizes and ellipticities with a widely used technique of fitting ellipses (e.g., Wozniak et al. [1991], Regan & Elmegreen [1997], Zheng et al. [2005], and Barazza et al. [2007] in the optical, and Knapen et al. [2000], Laine et al. [2002], Laurikainen et al. [2002], Sheth et al. [2000, 2002, 2003], and Marinova & Jogee [2007] in the NIR) to the full two-dimensional light distribution of the spirals in our 2MASS sample.

2MASS is one of the largest and most homogeneous NIR surveys. It allows us to measure the local bar fraction and characterize the bar properties and their relationship to their disks. This work provides a local anchor for studies of the evolution of the bar fraction with redshift.

2. OBSERVATIONS AND ANALYSIS

2.1. *Defining a Local Sample*

2MASS imaged the entire sky in the NIR bands, *J* (1.2 μm), *H* (1.6 μm), and K_s (2.2 μm) down to a limiting sensitivity of 21.6, 20.6, and 20.0 mag arcsec^{-2} (1 σ), respectively, with a typical angular resolution of $\sim 2''-3''$. From the image data set, which contains galaxies with $K_s < 14$ mag, Jarrett et al. (2003) assembled the LGA. The LGA consists of individual and co-added (to improve S/N) *J*-, *H*-, and K_s-band images of over 500 large galaxies imaged in the 2MASS, with sizes ranging from $2'$ to 2°.

In the absence of an established NIR morphological classification system, we used the optical RC3 morphological classification for our sample selection. We selected all 339 LGA galaxies with good S/N that were identified as spirals (S0/a–Sd) in the RC3. From these, we excluded 165 highly inclined galaxies ($i > 65^\circ$, where inclination is derived from the disk axial ratio). We excluded galaxies classified as irregulars, mergers, or otherwise strongly interacting. We also limited our sample to the 151 closest galaxies ($D \lesssim 40$ Mpc) so that we may easily resolve potential bars. Distances to these spirals were taken from the NASA Extragalactic Database (NED). The median distance of our sample of galaxies is 18 Mpc. There is an inherent bias toward large, massive, and bright galaxies in 2MASS because it is relatively shallow (see Fig. 1). The list of galaxies selected and their global properties are listed in Table 1.

2.2. *The Bar Signature*

We detect the presence of a bar within a galaxy disk from the ellipticity and position angle (P.A.) profiles traced by the galaxy isophotes. We applied the IRAF task `ellipse` (Jedrzejewski

TABLE 1

2MASS Spiral Sample

Galaxy	α(J2000.0)[a] (hr)	δ (J2000.0)[a] (deg)	K_{abs} (mag)	K[b] (mag)	D[c] (Mpc)	R_{25}[a] (kpc)	i[a] (deg)	P.A.[a] (deg)
			S0/a Spirals					
NGC 1291	3.289	−41.108	−24.67	5.66	11.6	17.12	33	156
NGC 1317	3.379	−37.103	−24.39	7.74	26.6	11.68	32	72
NGC 1326	3.399	−36.464	−23.93	7.45	18.9	12.04	49	67
NGC 2217	6.361	−27.234	−24.67	7.09	22.5	16.19	28	0[d]
NGC 2681	8.892	51.313	−22.45	7.43	9.5	5.02	0	3[e]
NGC 2655	8.927	78.224	−24.49	6.95	19.5	13.63	54	16
NGC 5101	13.363	−27.430	−24.91	7.16	25.8	21.83	40	124
			Sa Spirals					
NGC 1022	2.642	−6.677	−23.09	8.44	20.2	7.53	46	68
NGC 1367	3.584	−24.934	−23.92	7.63	20.4	17.59	51	134
NGC 3169	10.237	3.466	−23.88	7.28	17.1	11.57	63	45
NGC 3718	11.543	53.068	−22.94	7.76	13.8	15.15	63	180
NGC 4314	12.376	29.895	−23.22	7.45	13.6	7.79	19	155[e]
NGC 4491	12.516	11.484	−19.31	9.88	6.9	1.61	64	147
NGC 5728	14.707	−17.253	−24.77	8.17	37.6	17.25	58	180
NGC 7172	22.034	−31.870	−24.45	8.32	35.7	11.76	58	105
NGC 7727	23.665	−12.292	−24.36	7.69	25.7	15.38	40	28[e]
			Sab Spirals					
NGC 1350	3.519	−33.629	−24.71	7.40	25.1	21.45	64	11
NGC 1398	3.648	−26.338	−24.96	6.50	19.5	21.26	45	100
NGC 1433	3.700	−47.222	−23.81	7.06	14.9	13.47	48	95
NGC 1512	4.065	−43.349	−23.00	7.49	12.5	18.55	61	56
NGC 2146	6.310	78.356	−23.40	7.06	12.4	9.91	58	123
NGC 2566	8.313	−25.499	−24.02	7.77	22.8	12.73	60	69
NGC 2775	9.172	7.038	−24.31	7.06	18.8	12.21	40	160
NGC 2985	9.840	72.280	−23.96	7.36	18.3	11.07	39	176
NGC 3049	9.914	9.272	−21.63	9.96	20.8	6.51	56	27
NGC 3031 (M81)	9.926	69.066	−24.84	3.83	5.4	17.83	63	157
NGC 3368 (M96)	10.779	11.820	−24.16	6.32	12.5	14.04	51	5
NGC 3898	11.821	56.084	−23.41	7.66	16.3	8.76	53	108
NGC 4151	12.176	39.406	−23.32	7.38	13.8	12.15	40	50
NGC 4448	12.471	28.621	−21.98	7.81	8.9	3.29	60	98
NGC 4450	12.475	17.085	−25.12	7.05	27.2	20.19	43	173
NGC 4750	12.835	72.875	−23.74	8.02	22.5	7.28	31	142
NGC 4725	12.841	25.501	−24.95	6.17	16.6	26.23	51	33
NGC 4736 (M94)	12.848	41.120	−24.66	5.11	9.0	16.55	30	105
NGC 4941	13.070	−5.552	−22.73	8.22	15.4	8.02	54	23
NGC 5317	13.888	33.491	−24.80	7.80	16.4	3.83	43	58
NGC 7217	22.131	31.359	−23.75	6.85	13.2	7.01	34	88
NGC 7552	23.270	−42.584	−24.18	7.54	22.1	11.94	51	103
			Sb Spirals					
NGC 210	0.676	−13.874	−23.39	8.39	22.7	15.63	54	163
NGC 488	1.363	5.257	−25.53	6.96	31.5	24.63	43	15
NGC 772	1.989	19.008	−25.47	7.20	34.1	35.23	59	131
NGC 986	2.559	−39.045	−24.42	7.78	27.6	15.84	57	28
NGC 1068	2.711	−0.013	−25.20	5.79	15.8	17.22	29	73
NGC 1097	2.772	−30.275	−24.98	6.25	17.7	25.59	51	140
NGC 1365	3.560	−36.141	−25.43	6.37	18.0	29.56	55	12
NGC 1530	4.391	75.296	−24.39	8.29	37.7	22.70	59	81
NGC 2090	5.784	−34.251	−22.50	8.05	12.9	11.31	64	17
NGC 3227	10.392	19.865	−23.39	7.64	16.0	11.56	59	157
NGC 3351	10.733	11.704	−23.50	6.67	10.8	11.95	57	13
NGC 3583	11.236	48.319	−23.98	8.38	29.7	10.23	55	134
NGC 3673	11.420	−26.737	−23.65	8.51	27.0	15.04	59	70
NGC 3675	11.436	43.586	−23.28	6.86	10.7	9.67	58	178
NGC 4102	12.107	52.711	−22.63	7.72	11.7	5.30	59	38
NGC 4501 (M88)	12.533	14.420	−26.24	6.27	31.7	31.28	60	138
NGC 4548 (M91)	12.591	14.496	−22.03	7.12	6.8	5.11	35	150

TABLE 1—*Continued*

Galaxy	α(J2000.0)[a] (hr)	δ (J2000.0)[a] (deg)	K_{abs} (mag)	K[b] (mag)	D[c] (Mpc)	R_{25}[a] (kpc)	i[a] (deg)	P.A.[a] (deg)
			Sb Spirals					
NGC 4579	12.629	11.818	−25.13	6.49	21.1	17.04	39	89
NGC 4593	12.661	−5.344	−24.71	7.99	35.6	15.42	55	38
NGC 4595	12.664	15.298	−19.69	10.03	7.7	1.87	52	110
NGC 5383	13.951	41.846	−23.93	8.54	33.2	12.79	38	107
NGC 5850	15.119	1.545	−24.65	8.10	35.6	22.24	41	107
NGC 5985	15.660	59.332	−24.57	8.15	35.0	26.16	64	15
NGC 6300	17.283	−62.820	−24.01	6.93	15.4	11.29	54	119
NGC 6902	20.408	−43.654	−24.33	8.61	38.7	29.01	43	158
NGC 7606	23.318	−8.485	−24.82	7.64	31.0	19.32	60	145
			Sbc Spirals					
NGC 289	0.878	−31.206	−23.78	8.00	22.6	18.05	40	129
NGC 613	1.572	−29.418	−24.54	7.03	20.6	16.28	50	119
NGC 1300	3.328	−19.411	−24.14	7.56	21.4	19.55	59	101
NGC 1566	4.333	−54.938	−24.71	6.89	20.8	26.42	44	32
NGC 1672	4.762	−59.248	−24.34	7.02	15.5	15.42	46	170[d]
NGC 2207	6.273	−21.373	−24.72	8.19	38.2	25.42	61	116
NGC 2336	7.451	80.178	−24.72	7.70	30.6	28.30	57	178
NGC 2442	7.607	−69.531	−24.65	6.87	20.1	15.72	50	23
NGC 2559	8.285	−27.457	−24.26	7.42	21.7	12.95	61	4
NGC 3344	10.725	24.922	−22.12	7.44	8.1	8.51	17	140[d]
NGC 3521	11.097	−0.035	−24.46	5.78	11.2	17.63	63	164
NGC 3642	11.372	59.074	−22.74	8.97	22.0	17.73	35	105
NGC 3882	11.768	−56.391	−23.71	8.31	25.4	9.40	55	107
NGC 3953	11.897	52.327	−23.78	7.05	14.6	16.29	63	13
NGC 3992 (M109)	11.960	53.375	−23.88	6.94	14.6	14.81	52	78
NGC 4051	12.053	44.531	−22.27	7.67	9.7	7.23	29	135
NGC 4303 (M61)	12.365	4.475	−24.85	6.84	21.8	19.65	19	162
NGC 4321 (M100)	12.382	15.823	−25.13	6.59	22.0	24.25	38	155[d]
NGC 4567 (VV 219B)	12.609	11.258	−24.19	8.30	31.5	12.58	43	88
NGC 4602	12.677	−5.133	−24.20	8.54	35.3	11.24	63	...
NGC 4639	12.715	13.257	−21.95	8.75	13.8	6.05	52	134
NGC 4930	13.068	−41.411	−23.94	8.83	35.9	24.19	46	44
NGC 5055 (M63)	13.264	42.029	−23.61	5.61	7.0	13.47	55	102
NGC 5054	13.283	−16.634	−24.33	7.59	24.2	16.87	54	171
NGC 5194 (M51A)	13.498	47.195	−23.54	5.50	6.4	9.22	47	163
NGC 5248	13.626	8.885	−23.77	7.25	16.0	13.24	50	125
NGC 5247	13.634	−17.884	−23.85	7.53	18.8	14.62	43	170
NGC 5371	13.928	40.462	−25.14	7.61	35.5	21.36	48	2
NGC 5347	13.937	5.015	−21.54	9.65	17.2	15.06	57	121
NGC 5713	14.670	−0.290	−23.77	8.33	26.3	10.42	40	12
NGC 5921	15.366	5.071	−23.47	8.10	20.5	13.02	44	140
NGC 6221	16.880	−59.216	−24.45	7.12	20.6	13.27	62	1
NGC 6384	17.540	7.061	−24.29	7.53	23.1	16.65	60	14
NGC 6744	19.163	−63.858	−24.40	5.94	11.7	35.54	49	16
			Sc Spirals					
NGC 578	1.508	−22.667	−23.19	8.59	22.6	15.30	54	115
NGC 628	1.612	15.783	−22.95	6.85	9.1	14.01	23	70[e]
NGC 864	2.258	6.002	−23.15	8.53	21.7	14.27	48	24
NGC 1073	2.728	1.376	−22.15	8.98	16.8	11.40	38	32
NGC 1084	2.767	−7.579	−23.52	7.93	19.5	8.94	52	35
NGC 1187	3.044	−22.868	−23.33	8.10	19.4	15.44	48	129
NGC 1232	3.163	−20.581	−24.46	7.38	23.4	24.44	30	99
NGC 1637	4.691	−2.857	−22.01	7.97	9.9	4.71	32	13
NGC 1809	5.035	−69.567	−21.95	9.35	18.2	3.05	51	143
NGC 2835	9.298	−22.356	−22.54	7.92	12.3	12.00	50	3
NGC 2997	9.761	−31.191	−24.48	6.41	15.1	21.56	46	97
NGC 2976	9.788	67.917	−20.43	7.52	3.9	3.28	61	143
NGC 3338	10.702	13.747	−23.16	8.13	18.1	10.74	55	100[f]
NGC 3359	10.777	63.224	−22.12	8.62	14.1	14.96	52	176
NGC 3486	11.007	28.975	−21.88	8.00	9.5	9.29	45	80
NGC 3614	11.306	45.748	−22.92	9.63	32.4	19.40	50	87

TABLE 1—*Continued*

Galaxy	α(J2000.0)[a] (hr)	δ (J2000.0)[a] (deg)	K_{abs} (mag)	K[b] (mag)	D[c] (Mpc)	R_{25}[a] (kpc)	i[a] (deg)	P.A.[a] (deg)
			Sc Spirals					
NGC 3631	11.351	53.169	−23.05	7.99	16.1	11.44	35	118
NGC 3726	11.556	47.029	−22.60	7.78	11.9	10.49	49	14
NGC 3938	11.880	44.122	−22.44	7.81	11.2	8.11	13	...
NGC 4254	12.314	14.417	−25.70	6.93	33.5	26.05	29	...
NGC 4535	12.572	8.198	−24.79	7.38	27.2	27.30	41	180
NGC 4647	12.726	11.583	−23.42	8.05	19.7	8.02	34	125
NGC 5236 (M83)	13.617	−29.865	v24.65	4.62	7.1	14.47	24	48[e]
NGC 5426	14.057	−6.067	−23.31	9.50	36.4	15.80	62	1
NGC 5427	14.057	−6.031	−24.21	8.59	36.4	15.19	42	
NGC 5643	14.545	−44.174	−23.94	7.17	16.7	11.97	30	88
NGC 6215	16.852	−58.993	−23.40	8.28	21.6	6.67	44	83
			Scd Spirals					
NGC 275	0.851	−7.066	−22.04	9.88	24.2	5.04	37	105
NGC 598 (M33)	1.564	30.660	−20.95	4.10	1.0	9.93	54	23
NGC 1494	3.962	−48.908	−21.15	9.82	15.6	7.90	64	1
NGC 2280	6.747	−27.639	−23.86	8.26	26.4	25.94	64	164
NGC 2283	6.765	−18.211	−21.46	8.83	11.4	6.33	43	175
NGC 2403	7.614	65.603	−21.56	6.19	3.6	12.09	60	126
NGC 2541	8.244	49.061	−19.36	10.09	7.8	6.55	62	167
NGC 3184	10.305	41.424	−22.35	7.23	8.2	9.38	17	...
NGC 3319	10.653	41.687	−19.99	10.07	10.3	8.75	59	37
NGC 4654	12.732	13.126	−23.05	7.74	14.4	10.49	58	122
NGC 5457 (M101)	14.053	54.348	−25.40	5.51	7.2	31.98	8	35[d]
NGC 5474	14.084	53.662	−16.89	9.48	1.9	1.21	42	79
NGC 6140	16.349	65.390	−20.76	9.74	12.6	8.95	37	76
NGC 6946	20.581	60.154	−23.40	5.37	5.7	9.37	30	62[d]
NGC 7418	22.943	−37.030	−22.99	8.52	20.1	11.45	41	139
NGC 7424	22.955	−41.071	−21.33	9.25	13.1	14.88	41	115[e]
			Sd Spirals					
NGC 300	0.915	−37.685	−20.66	6.38	2.6	7.50	48	114
NGC 337	0.997	−7.578	−22.70	9.10	22.9	9.61	53	60
NGC 925	2.455	33.579	−21.56	7.87	7.7	12.60	57	102
NGC 1313	3.304	−66.497	−21.46	7.57	6.4	8.60	40	39
NGC 4145	12.167	39.884	−22.26	8.48	14.1	11.67	55	100
NGC 4519	12.558	8.655	−21.59	9.56	17.0	7.07	37	149
NGC 5068	13.315	−21.039	−22.30	7.55	9.3	10.11	26	110[d]
NGC 5585	14.330	56.729	−19.89	9.50	7.5	6.06	53	32
NGC 5556	14.343	−29.242	−21.86	9.55	19.2	11.82	48	143
NGC 7320	22.601	33.948	−19.64	10.52	15.3	4.25	55	133
NGC 7793	23.964	−32.591	−21.15	6.86	4.0	5.91	58	84

NOTE.—Table 1 is also available in machine-readable form in the electronic edition of the *Astrophysical Journal*.
[a] HyperLeda Extragalactic Database (LEDA).
[b] 2MASS search engine GATOR.
[c] NED.
[d] Martin (1995).
[e] 2MASS IRSA.
[f] Heraudeau & Simien (1996).

1987) on the combined $J + H + K_s$ LGA images for all the galaxies in our sample, with a step size of 3″ (the 2MASS angular resolution). The transition from the (round) bulge-dominated center to the disk is typically characterized by an increase in ellipticity, $\epsilon = 1 - (b/a)$. For a disk or a bar, the P.A. remains constant unless there are spiral arms, which force the P.A. to change continuously. In absence of these arms, the ellipticity increases monotonically at a constant P.A. within the bar region. At the end of the bar, the ellipticity drops abruptly and the P.A. changes sharply as the isophotes transition from the bar into the disk. An example of what we term an ideal "bar signature" is shown in Figure 2 for NGC 1300. In this case, within the bar region, the bar isophotes show a continuous increase in ellipticity, maintaining a constant P.A. At the end of the bar, the ellipticity of the image isophotes decreases and the P.A. changes sharply, denoting the difference between the bar and the disk P.A. Cases in which the bar and the disk have the same P.A. are discussed below.

The change in ellipticity and the change in P.A. are moderated by the spiral arms that may retard the corresponding P.A. drop to occur further out in the disk, outside the bar region. For this reason we choose the semimajor axis (SMA) of the isophote with maximum ellipticity (ϵ_{max}) to be the size of the bar, a_{bar}. Due to

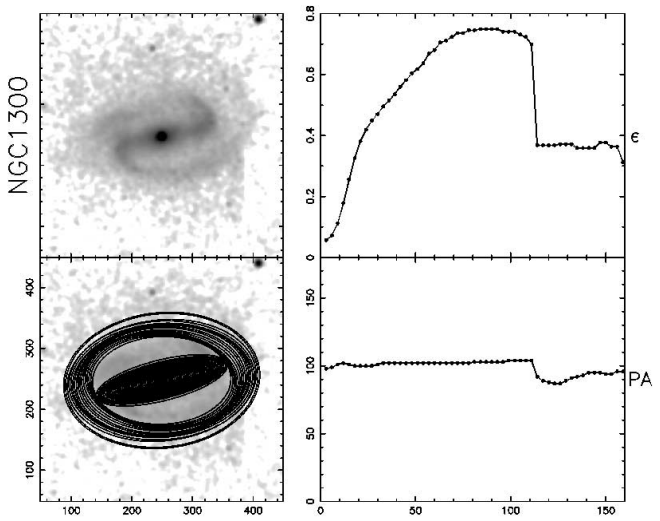

FIG. 2.—*Top left:* 2MASS $J + H + K_s$ combined image of NGC 1300. *Bottom left:* NIR image of NGC 1300 with ellipse-fit ellipses overplotted. *Top right:* Ellipticity profile for NGC 1300. *Bottom right:* P.A. profile for NGC 1300. This is the bar signature in NGC 1300: ϵ increases monotonically and drops abruptly with $\Delta\epsilon > 0.1$, as ellipses conform to the disk isophotes. The position angle stays constant within the bar region and changes, with ΔP.A. $> 10^\circ$, when the end of the bar is reached.

spiral arms, the ellipticity peak is often broadened into a "flat field" (see Fig. 2). To account for the uncertainty in defining which SMA corresponds to the maximum ellipticity, we characterize the error in the bar size measurement by the SMA range encompassing the tip of the ellipticity peak in the bar signature, over which $\epsilon \gtrsim (\epsilon_{\max} - \delta\epsilon)$, where we chose $\delta\epsilon = 0.01$.

In order to automate our bar identification method, we required a bar to have a projected ellipticity, $\epsilon_{\max}$, greater than 0.2, and the end of the bar to be marked by a change in ellipticity, $\Delta\epsilon > 0.1$, with an accompanying change in the position angle, ΔP.A. $> 10^\circ$. We do not identify a bar signature in the first three points of the ellipticity profile, which corresponds to 3 times the PSF FWHM (9″). More than 95% of all bars in our sample are longer than 5 times the PSF FWHM. Therefore, a more realistic threshold to our bar detection method for identifying bars is 15″, which corresponds to 1.3 kpc at the median distance of 18 Mpc in our sample. This size scale makes this study an ideal comparison sample for high-redshift galaxies where similar spatial resolution is typically achieved. We discuss this issue in more detail in § 3.2.1. Our reason for choosing $\epsilon > 0.2$ is to distinguish between bars and oval structures (e.g., flattened bulges or inner disks). Our choices for the $\Delta\epsilon$, ΔP.A. are based on previous studies which have used these criteria to identify bars (Knapen et al. 2000; Laine et al. 2002; Sheth et al. 2003).

Some of the galaxies in our sample have ellipticity profiles that conform to the bar signature described above, but have P.A. profiles that do not.[5] Visual inspection of these images shows that some appear to contain a bar, while others do not. These cases require special consideration as discussed here and illustrated in Figure 3*a*–3*e*. The P.A. profiles of these galaxies deviate from the P.A. bar signature in one of two ways: (1) the change in P.A. that accompanies the drop in ellipticity is less than 10°, or (2) the P.A. varies continuously within the region where there is a monotonic increase in ellipticity.

There are two possibilities for the first case: (*a*) a bar is present, but it has a P.A. similar to that of the disk (e.g., Fig. 3*a*); or (*b*) there is no bar and the barlike ellipticity signature traces the presence of an inner disk embedded within the galaxy disk (e.g., Fig. 3*b*). Since bars are expected to be randomly oriented with respect to the underlying disk and ΔP.A. may vary within $0^\circ \lesssim \Delta\text{P.A.} \lesssim 90^\circ$, we expect that, based strictly on geometric considerations, ~10% of bars will have a P.A. within 10° of the host galaxy disk P.A.

In the second case, the P.A. does not remain constant within the region where the ellipticity increases monotonically, but varies continuously. Two scenarios are responsible for this behavior, both involving the presence of spiral arms: (*a*) spiral arms originating within the bar region twist the bar isophotes, producing a progressive change in P.A. like the example shown in Figure 3*c*; or (*b*) no bar is present but the ellipticity profile is instead produced by the progressive stretching of disk isophotes by fairly open, bright spiral arms. This is shown in Figure 3*d*.

If we were to consider solely the ellipticity signature, all of the cases with these different P.A. signatures would be classified as barred galaxies, even though they probably do not all host bars. Instead, we adopt a separate category for these galaxies, introduced by Sheth et al. (2003): we classify these galaxies as candidate barred spirals and will hereafter be referred to as "candidates." We visually inspected each individual candidate to determine whether a real bar was present or not. Candidates for which the ellipticity signature is produced by spiral arms (Fig. 3*d*) or an inner disk (Fig. 3*b*) are classified as "unbarred." The remaining candidates are classified as barred.

Galaxies that do not show a monotonic rise and fall in ellipticity are classified as "unbarred" galaxies. An example of an unbarred galaxy is shown in Figure 3*e*, the nearby spiral, M88.

3. RESULTS

3.1. *Bar Fraction*

We successfully applied the ellipse-fit technique to the 151 galaxies in our sample. We found that 89 (59%) of all galaxies in our sample display both an ellipticity and P.A. bar signature, and are therefore identified *clearly* as barred spirals. This fraction represents a lower limit to the NIR bar fraction measured in our 2MASS sample. Of the candidate barred spirals, where only one of the two bar signatures is present, 12/22 appear to have bars on visual inspection. Thus, the fraction of galaxies with bars in our 2MASS sample increases to 101/151 (67%). For the remainder of the paper, we refer to this 67% sample as "barred spirals." Our classification and notes for each galaxy, as well as their RC3 classifications are presented in Table 2.

We identify 85% of all SB galaxies and 80% of all SAB galaxies from the RC3 as barred spirals (see Table 2). In addition, we classify 11 galaxies within the RC3 SA category as barred spirals. With our exclusion of highly inclined galaxies ($i > 65^\circ$), our sample has 64 galaxies in common with those of E2000. Our classification agrees in 85% of the cases with the visual classification by E2000. Most of the RC3 and E2000 SB and SAB galaxies that do not meet our bar identification requirement either have bars that are too small, or have insufficient change in the ellipticities due to open spiral arms and/or disks with higher ellipticites than the bar; two such examples are NGC 6140 and NGC 2146 shown in Figures 3*f* and 3*g*.

Following our adopted definition for the bar signature, there are a number of instances in which our method fails to identify bars (see § 2.2). Our measurement of the bar fraction is thus a firm lower limit to the true value, but it is not straightforward to quantify the error in the local bar fraction. Poisson statistics would indicate an error of ±2% on the total bar fraction of 67%.

[5] In our sample, 15% (22/151) of all spirals fell into this category.

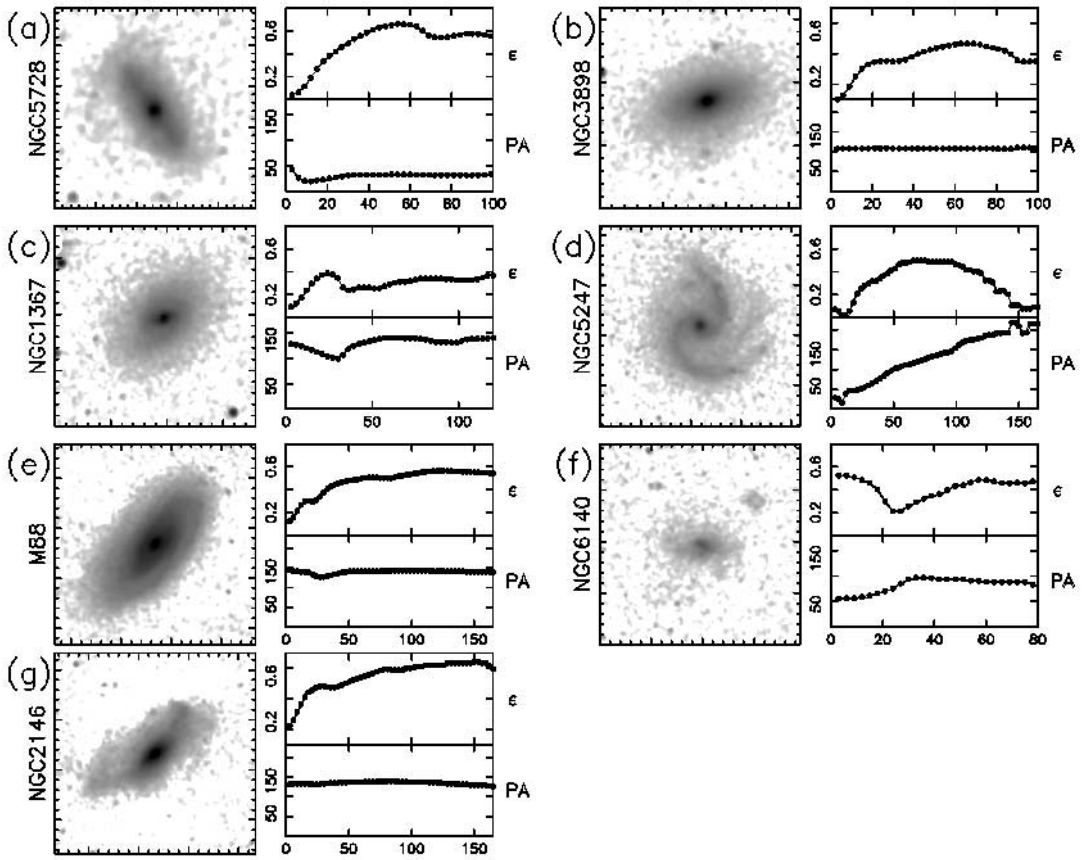

FIG. 3.—Ellipse-fit results following the same format as Fig. 2, excluding image with ellipses overplotted. (*a*) NGC 5728 is classified as a candidate, but contains a bar with P.A. equal to that of the disk. (*b*) NGC 3898 displays a P.A. profile similar to that of candidate NGC 5728, but here it corresponds to a bright inner disk: it is not barred. (*c*) NGC 1367 is a candidate that contains a bar, even though its P.A. profile displays a continuous change in P.A. within the bar region. This is due to the presence of spiral arms, which result in the twisting of the bar isophotes within the bar region. (*d*) NGC 5247 is an example of a candidate in which the presence of spiral arms may mimic a bar ellipticity signature: it is not barred. (*e*) M88 is an unbarred galaxy that shows no sign of bar presence in its ellipticity profile. (*f*) NGC 6140 is a spiral classified as strongly barred (SB) in the RC3, whose bar is smaller than our detection limit of 15″. Ellipse-fit of its 2MASS NIR image does not trace the ellipticity increase associated to the bar. (*g*) NGC 2146 is another SB spiral (RC3) for which our method fails to recognize its bar. Following the ellipticity monotonic increase characteristic of a bar signature, instead of dropping sharply, the ellipticity of the galaxy increases further due to the presence of an open-angle spiral arm.

3.2. *Bar Properties*

3.2.1. *Bar Sizes*

We define the relative bar size, $a_{\rm bar}/R_{25}$, as the ratio of the bar deprojected semimajor axis to the RC3 radius of the host galaxy at a B magnitude of 25 (R_{25}). The bar relative size has the advantage of being a distance-independent measure. The error on the relative bar size is $\sim$10% and is dominated by the uncertainty on the measurement from the ellipticity profile of the bar signature. We found that $\sim$90% of all bars within the sample extend out to less than 50% of their host galaxy disk. Bars with the largest relative sizes are mostly found in small early-type galaxies (see Fig. 4) with $R_{25} \lesssim 23$ kpc. The properties of the typical 2MASS bar are summarized in Table 3.

We find a clear trend of bar sizes, both in terms of $a_{\rm bar}$ and $a_{\rm bar}/R_{25}$, along the Hubble sequence, with early-type bars being significantly larger than late types (see Fig. 5). Bars in early Sa–Sb spirals have a median $a_{\rm bar}/R_{25} = 0.43 \pm 0.04$, while bars in later type Sc–Sd spirals have a median $a_{\rm bar}/R_{25} = 0.2 \pm 0.02$, making the median relative bar size in early-type galaxies larger than in late types by a factor of 2. Note that the low median value for the S0/a spirals is probably due to the low number of these transitional lenticular-to-spiral galaxies in our sample. Furthermore, the sizes of early-type bars cover a large range in relative sizes, $0.1 \lesssim a_{\rm bar}/R_{25} \lesssim 0.9$, while late-type bars are restricted to lower relative sizes, $a_{\rm bar}/R_{25} \lesssim 0.5$.

The distribution of absolute sizes of bars is dependent on resolution and the galaxy population being probed. The 2MASS sample probes the largest, brightest and most massive galaxies in the local universe. Figure 6*a* presents our 2MASS bar sizes as a function of distance. The median bar semimajor axis for the subset of barred spirals at a distance $D \lesssim 14$ Mpc is 1.2 kpc. As we include more distant galaxies, the median bar size increases up to $\sim$3.5 kpc (for $D \lesssim 40$ Mpc); this trend parallels the limit of bar size detection of $\gtrsim$15″. The population of bars being probed is thus affected by the bar detection limit. We must, therefore, take into account the bar size for a proper determination of the bar fraction. Figure 6*b* shows how the 2MASS bar fraction changes depending on the ability to detect a particular bar size. This is especially important for studies of bars at high redshifts as discussed further in §§ 4.4 and 4.5.

3.2.2. *Bar Strengths*

The higher the true ellipticity of the bar, the greater the effect of the bar potential on the otherwise axisymmetric gravitational potential of the disk. The maximum deprojected ellipticity thus provides a simple assessment of the bar strength. It has been shown to correlate well with other strength measures, such as

TABLE 2
2MASS BARS

Galaxy	Type (RC3)[a]	ϵ_{max}	P.A.$_{bar}$ (deg)	$a \pm \delta a$[b] (arcsec)	a_{deproj} (arcsec)	a_{bar} (kpc)	a_{bar}/R_{25}
			Barred				
S0/a spirals:							
NGC 1291	SB0/a	0.40	171	87 ± 5	88	5.0	0.29
NGC 1317	SAB(rl)0/a	0.24	150	42 ± 2	49	6.3	0.54
NGC 1326	SB(rl)0/a	0.37	20	30 ± 3	39	3.6	0.30
NGC 2217	SB(rs)0/a	0.43	113	39 ± 2	43	4.7	0.29
NGC 2681	SAB(rs)0/a;Sy	0.21	77	18 ± 2	18	0.8	0.16
NGC 2655	SAB(s)0/a	0.32	85	33 ± 5	53	5.0	0.37
NGC 5101	SB(rl)0/a	0.51	122	48 ± 3	48	6.0	0.28
Sa spirals:							
NGC 3718	SB(s)a;pec;Sy1	0.20	12	60 ± 3	65	4.3	0.29
NGC 4314	SB(rs)a	0.63	148	69 ± 8	69	4.6	0.59
NGC 4491	SB(s)a:	0.54	138	24 ± 3	25	0.8	0.52
NGC 7172	Sa_pec_Sy2	0.51	96	45 ± 5	46	8.0	0.68
NGC 7727	SAB(s)a_pec	0.21	87	27 ± 2	33	4.2	0.27
Sab spirals:							
NGC 1350	SB(r)ab	0.55	36	51 ± 5	68	8.3	0.39
NGC 1398	SB(rs)ab;Sy	0.33	12	39 ± 2	55	5.2	0.25
NGC 1433	SB(rs)ab_Sy2	0.62	96	90 ± 8	90	6.5	0.48
NGC 1512	SB(r)ab	0.64	44	72 ± 3	77	4.7	0.25
NGC 4450	SA(s)ab	0.50	6	42 ± 3	43	5.7	0.28
NGC 4725	SAB(r)ab;pec	0.65	48	132 ± 9	139	11.2	0.43
NGC 4941	SAB(r)ab_Sy2	0.53	16	93 ± 6	94	7.1	0.88
NGC 5317	SA(rs)bc;pec	0.43	47	36 ± 3	37	2.9	0.76
NGC 7552	SB(s)ab	0.59	96	48 ± 3	48	5.2	0.43
Sb spirals:							
NGC 1097	SBb;Sy1	0.61	147	87 ± 6	88	7.5	0.29
NGC 1365	SBb(s)b;Sy1.8	0.59	85	90 ± 5	152	13.3	0.45
NGC 3227	SAB(s);pec;Sy	0.59	151	57 ± 8	58	4.5	0.39
NGC 772	SA(s)b	0.24	116	21 ± 3	23	3.8	0.11
NGC 986	SB(rs)b	0.63	58	48 ± 6	61	8.1	0.51
NGC 1068	SA(rs)b;Sy1;2	0.33	48	15 ± 2	15	1.2	0.07
NGC 1530	SB(rs)b	0.61	124	51 ± 2	77	14.0	0.62
NGC 3351	SB(r)b;HII	0.43	113	57 ± 3	103	5.4	0.45
NGC 3583	SB(s)b	0.40	76	21 ± 2	33	4.8	0.47
NGC 3673	SB(r)b	0.68	83	45 ± 3	48	6.3	0.42
NGC 4548 (M91)	SBb(rs);Sy	0.49	60	57 ± 2	70	2.3	0.45
NGC 4579	SAB(rs)b;Sy1.9	0.46	59	39 ± 3	42	4.3	0.25
NGC 4593	SB(rs)b_Sy1	0.59	58	48 ± 5	53	9.2	0.60
NGC 5383	SB(rs)b:pec	0.57	127	48 ± 5	50	8.0	0.63
NGC 5850	SB(r)b	0.60	117	60 ± 3	61	10.5	0.47
NGC 5985	SAB(r)b;Sy1	0.59	15	48 ± 3	48	8.1	0.31
NGC 6300	SB(rs)b	0.45	71	36 ± 5	52	3.9	0.34
Sbc spirals:							
NGC 289	SAB(rs)bc	0.48	122	21 ± 2	21	2.3	0.13
NGC 613	SB(rs)bc	0.70	124	75 ± 9	75	7.5	0.46
NGC 1300	SB(s)bc	0.75	103	84 ± 9	84	8.7	0.45
NGC 1566	SAB(rs)bc;Sy1	0.38	3	33 ± 2	36	3.7	0.14
NGC 1672	SB(r)bc_Sy2	0.63	96	72 ± 6	102	7.7	0.50
NGC 2559	SB(s)bc_pec:	0.53	39	27 ± 2	39	4.1	0.32
NGC 3344	SAB(r)bc	0.28	2	24 ± 2	25	1.0	0.11
NGC 3882	SB(s)bc	0.57	124	33 ± 2	36	4.4	0.47
NGC 3953	SB(r)bc	0.47	46	27 ± 2	40	2.9	0.18
NGC 3992 (M109)	SB(rs)bc;LINER	0.60	39	51 ± 5	65	4.6	0.31
NGC 4051	SAB(rs)bc	0.65	134	63 ± 3	63	3.0	0.41
NGC 4303 (M61)	SAB(rs)bc;HII	0.59	3	48 ± 3	48	5.1	0.26
NGC 4321 (M100)	SAB(s)bc;LINER	0.51	106	57 ± 3	66	7.0	0.29
NGC 4639	SAB(rs)bc	0.47	169	24 ± 3	30	2.0	0.33
NGC 4930	SB(rs)bc	0.56	43	42 ± 2	42	7.3	0.30
NGC 5054	SA(s)bc	0.31	162	21 ± 2	21	2.5	0.15
NGC 5194 (M51A)	SA(s)bc	0.27	139	15 ± 2	16	0.5	0.06
NGC 5371	SAB(rs)bc	0.30	94	24 ± 5	36	6.1	0.29
NGC 5347	SB(rs)ab_Sy2	0.53	103	30 ± 2	33	2.8	0.18
NGC 5713	SAB(rs)bc;pec	0.45	104	18 ± 2	23	3.0	0.29

TABLE 2—*Continued*

Galaxy	Type (RC3)[a]	ϵ_{max}	P.A.$_{bar}$ (deg)	$a \pm \delta a$[b] (arcsec)	a_{deproj} (arcsec)	a_{bar} (kpc)	a_{bar}/R_{25}
NGC 5921	SB(r)bc	0.58	16	39 ± 3	50	5.0	0.38
NGC 6221	SB(s)bc;pec;Sy2	0.43	117	24 ± 2	47	4.7	0.35
NGC 6384	SAB(r)bc	0.50	35	24 ± 2	28	3.2	0.19
NGC 6744	SAB(r)bc	0.68	179	90 ± 8	95	5.4	0.15
Sc spirals:							
NGC 578	SAB(rs)c	0.53	84	18 ± 2	22	2.4	0.16
NGC 864	SAB(rs)c	0.44	102	24 ± 2	35	3.7	0.26
NGC 1073	SB(rs)c	0.66	59	45 ± 3	48	3.9	0.34
NGC 1187	SB(r)c	0.56	134	36 ± 3	36	3.4	0.22
NGC 1232	SAB(rs)c	0.42	86	21 ± 3	21	2.4	0.10
NGC 1637	SAB(rs)c	0.43	68	24 ± 3	27	1.3	0.28
NGC 2835	SAB(rs)c	0.41	115	21 ± 2	31	1.9	0.15
NGC 3359	SB(rs)c	0.68	7	42 ± 5	43	2.9	0.20
NGC 3486	SAB(r)c	0.39	73	21 ± 2	21	1.0	0.10
NGC 3614	SAB(r)c	0.39	87	27 ± 2	27	4.2	0.22
NGC 3631	SA(s)c	0.40	13	51 ± 6	61	4.8	0.42
NGC 3726	SAB(r)c	0.70	31	39 ± 3	41	2.4	0.23
NGC 4535	SAB(s)c	0.62	37	45 ± 9	51	6.7	0.25
NGC 4647	SAB(rs)c	0.21	88	21 ± 2	23	2.2	0.27
NGC 5236 (M83)	SAB(s)c;Sbrst	0.56	58	114 ± 5	114	4.0	0.27
NGC 5643	SAB(rs)c	0.65	84	54 ± 5	54	4.4	0.36
Scd spirals:							
NGC 2283	SB(s)cd	0.55	173	12 ± 2	12	0.7	0.11
NGC 2403	SAB(s)cd	0.41	113	15 ± 2	16	0.3	0.02
NGC 5457 (M101)	SAB(rs)cd	0.45	82	51 ± 2	51	1.8	0.06
NGC 6946	SAB(rs)cd	0.46	17	60 ± 2	65	1.8	0.19
NGC 7418	SAB(rs)cd	0.61	126	30 ± 2	31	3.0	0.26
NGC 7424	SAB(rs)cd	0.51	130	18 ± 3	18	1.2	0.08
Sd spirals:							
NGC 337	SB(s)d	0.45	162	21 ± 6	35	3.9	0.40
NGC 1313	SB(s)d	0.59	15	33 ± 9	35	1.1	0.13
NGC 4145	SAB(rs)d;LINER	0.34	135	12 ± 3	16	1.1	0.09
NGC 5068	SB(s)d	0.55	149	21 ± 3	22	1.0	0.10
NGC 5556	SAB(rs)d	0.48	93	15 ± 2	20	1.8	0.16
			Barred Candidates				
Sa spirals:							
NGC 1022	SB(s)a;Sbrst	0.42	108	18 ± 2	22	2.1	0.28
NGC 1367	SABa	0.39	104	24 ± 2	28	2.8	0.16
NGC 5728	SAB(r)a;Sy2	0.66	33	54 ± 3	72	13.0	0.76
Sab spirals:							
NGC 4151	SAB(rs)ab	0.48	132	63 ± 5	82	5.5	0.45
Sb spirals:							
NGC 210	SAB(s)b	0.47	173	33 ± 3	34	3.7	0.24
NGC 7606	SA(s)b	0.61	142	36 ± 5	36	5.4	0.28
Sbc Spirals							
NGC 2207	SAB(rs)bc_pec	0.42	64	24 ± 3	42	7.7	0.30
NGC 4567 (VV 219B)	SA(rs)bc	0.45	58	30 ± 6	33	5.1	0.40
Sc spirals:							
NGC 2976	SAc;pec	0.69	137	72 ± 5	73	1.4	0.42
Scd spirals:							
NGC 275	SB(rs)cd_pec	0.35	78	12 ± 3	13	1.5	0.30
NGC 1494	SAB(rs)cd	0.47	174	15 ± 3	16	1.2	0.15
NGC 2280	SA(s)cd	0.60	153	48 ± 3	52	6.7	0.26

NOTE.—Table 2 is also available in machine-readable form in the electronic edition of the *Astrophysical Journal*.

[a] As given in NED.

[b] Error in measurement; see § 2.2.

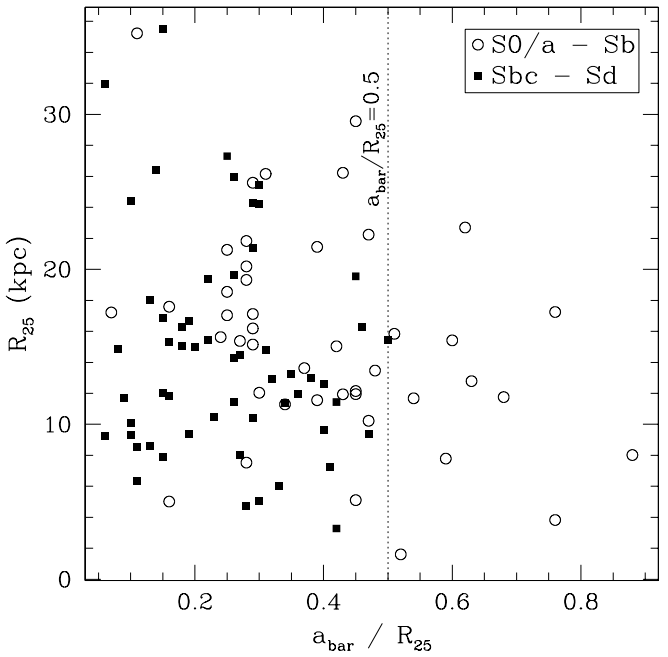

FIG. 4.—Plot of a_{bar}/R_{25} as a function of R_{25}. Symbols for early-type and late-type spirals follow the same convention as Fig. 1. Note that ~90% of all bars extend out to less than half of the underlying disk radii and the bars largest with respect to the blue disk of their host galaxy are mostly found in the smaller early-type galaxies.

the Q_b-parameter (Block et al. 2004; Laurikainen et al. 2002), which characterizes the bar strength by measuring the maximum gravitational bar torque relative to the galactic disk (Buta & Block 2001).

The typical bar in our sample has a projected ellipticity of 0.5. We find that the distribution of ellipticities, shown in Figure 7*a*, is clearly skewed toward higher ellipticities, with a sharp drop in bar population around $\epsilon \sim 0.75$. By definition, our bar detection method excludes bars with $\epsilon \lesssim 0.2$, which explains the absence of these very weak bars. Since highly elliptical bars are the easiest to identify with our ellipse-fit method, the sharp decline in Figure 7*a* is an intrinsic property of bars, indicating a lack of very strong bars in the local universe. We discuss this in more detail in § 4.2.

We find a weak correlation between the bar strength and the bar size, both in terms of a_{bar} and a_{bar}/R_{25}, as shown in Figure 7*b*. For all barred spirals in our sample we find that bar ellipticity and relative size are correlated with a ~0.99 level of significance as determined from the correlation *r*-coefficient of 0.34. Stronger bars appear to also be the longest ones, both in absolute size and relative to the host disk. This trend is more significant for early-type barred galaxies; the correlation coefficient for early types is $r = 0.46$, compared to $r = 0.22$ for late types. Previous studies (Martin 1995; Laurikainen et al. 2002; Erwin 2005) found no significant correlation between these two bar properties, although Laurikainen et al. (2002) noted a slight increase in bar length with increasing bar strength when considering only late-type galaxies. We find that the bar ellipticity is not correlated with the Hubble type, the galaxy size or the *K*-band luminosity.

4. DISCUSSION

4.1. *Bar Fractions in the Optical and NIR*

Observations in the NIR provide a better discriminant between barred and unbarred spirals than in the optical. The RC3 classification is based on the presence of a bar as seen in blue photographic plates: spirals in which a bar is clearly present were classified as strongly barred (SB), while the bars in SAB galaxies were referred to as "weak bars" or "oval distortions" because they are a minor distortion to the disk. In our NIR analysis, all the intermediate SAB galaxies are classified as barred. We do not make a distinction such as the SB and the SAB classification; galaxies are either barred or unbarred.

TABLE 3
LOCAL BAR PROPERTIES

Property[a]	2MASS Bar (S0/a–Sd)	Early-Type 2MASS Bar (Sa–Sb)	Late-Type 2MASS Bar (Sc–Sd)
a_{bar} (kpc).....	4.2 ± 2.9	5.4 ± 3.3	2.2 ± 1.7
a_{bar}/R_{25}.....	0.29 ± 0.17	0.43 ± 0.18	0.22 ± 0.11
ϵ_{bar}	0.50 ± 0.13	0.54 ± 0.13	0.48 ± 0.12

[a] Median value ±1 σ standard deviation.

Our lower limit to the NIR bar fraction of 0.59 is conservative because it is restricted to barred galaxies with both an ellipticity and P.A. signature. It is consistent with the bar fraction of 59% found by L2004, who apply a Fourier decomposition method to a sample of 158 OSUBSGS and 22 2MASS spirals with inclination $i \lesssim 65^\circ$. The recent analysis by Marinova & Jogee (2007), using 136 OSUBSGS with inclination $i < \sim 60^\circ$, further confirm our result with a measured local *H*-band bar fraction at 58%.

The NIR bar fraction increases to 0.67 when we include the barred galaxies with only the ellipticity signature. We compare this result to the total fraction of 0.63 (SB+SAB) in the RC3 *B*-band analysis. Although the relative fraction of strong (SB) or weak bars (SAB) changes based on the wavelength of observation, the overall fraction of barred galaxies remains relatively unchanged from the *B* band to the *K* band. This indicates that the bar morphology, although degraded, can be reliably detected by eye in the *B* band. We note that it may be likely that fewer galaxies in the *B* band are identified as bars by automated algorithms due to the more irregular or patchy appearance of galaxies in bluer bands. Algorithms such as the ellipse-fitting algorithm rely on a smooth light distribution and often fail for irregular distributions. Recent work by Barazza et al. (2007) explores the local bar fraction in the optical using this algorithm on galaxies from the Sloan Digital Sky Survey.

Our results are consistent with the *H*-band bar fraction of 0.72 measured by E2000 in their OSUBGS sample. In contrast to our approach, E2000 did not make selection cuts based on inclination to restrict their sample and, like earlier optical studies (e.g., RC3), relied on visual inspection to identify bars. W2002 report a slightly larger *H*-band bar fraction of 0.79 in their sample of 72 OSUBSGS galaxies with inclination $i \lesssim 60^\circ$. However, even though this method is quantitative it is based on the selection of only two ellipses, an inner and outer one, to define a bar. The ellipse fitting method used here is more robust because it uses the full two-dimensional light distribution.

Our method does not detect bars in $\sim\frac{1}{3}$ of our sample. There are a number of reasons why our method may have failed to detect an existing bar, particularly a small bar (see § 3.1). However, this is unlikely to be the case in a majority of the galaxies we classify as unbarred spirals (e.g., Fig. 3*e*). Models suggest that a bar may be prevented from forming if the disk is too dynamically hot, or if the disk is not sufficiently massive (Ostriker & Peebles 1973; Athanassoula et al. 2005). Galaxies may also dissolve their bars by accumulating a large central mass concentration or by undergoing a merger (Combes & Gerin 1985; Das et al. 2003; Shen & Sellwood 2004). In either case, an unbarred spiral should

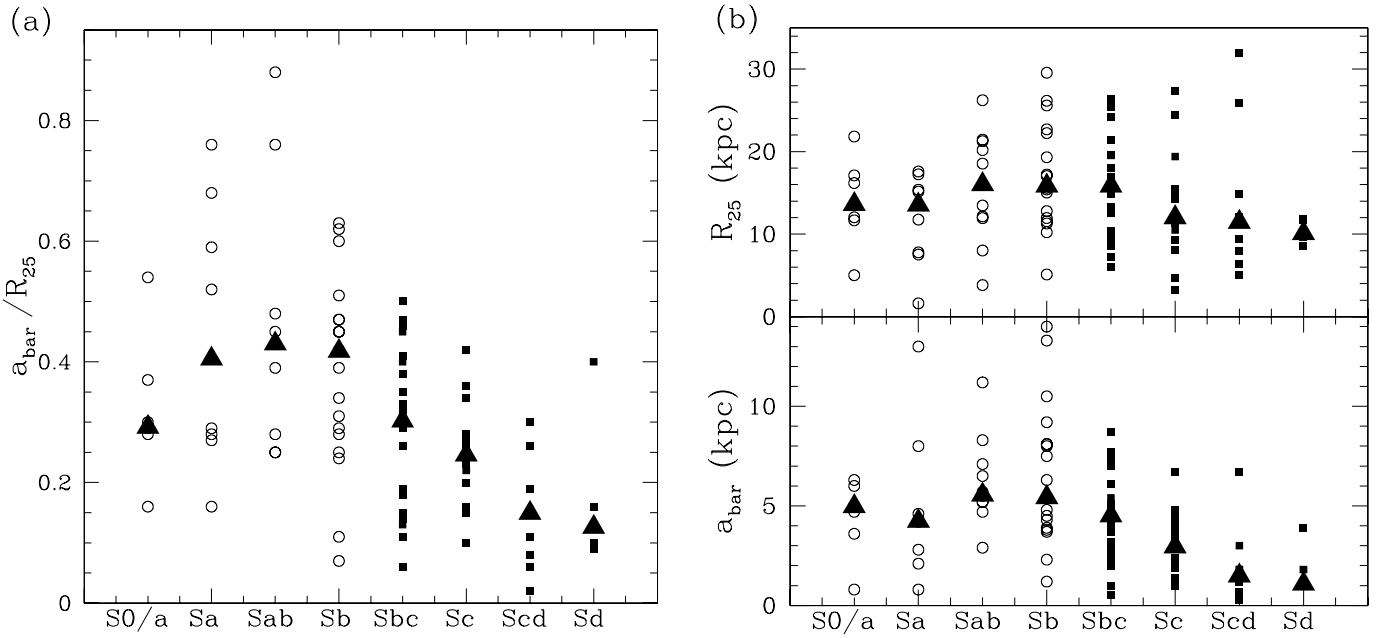

FIG. 5.—(*a*) Plot of a_{bar}/R_{25} as a function of Hubble type. Symbols for early-type and late-type spirals follow the same convention as Fig. 1. Filled triangles show median values for each Hubble type. A clear trend shows that early-type bars tend to be generally larger than late-type (Sbc–Sd) bars. S0/a bars have a smaller median size than that expected from the trend of bar sizes along the Hubble sequence. However, this is likely due to the low number of objects that we have in this category. (*b*) Same as (*a*), but for R_{25} (*top*) and a_{bar} (*bottom*). Note that both a_{bar} and R_{25} tend to be smaller for late-type spirals. This confirms that the trend of smaller relative sizes in late-type spirals, shown in (*a*), is driven by bars being intrinsically smaller in late-type spirals than in early types.

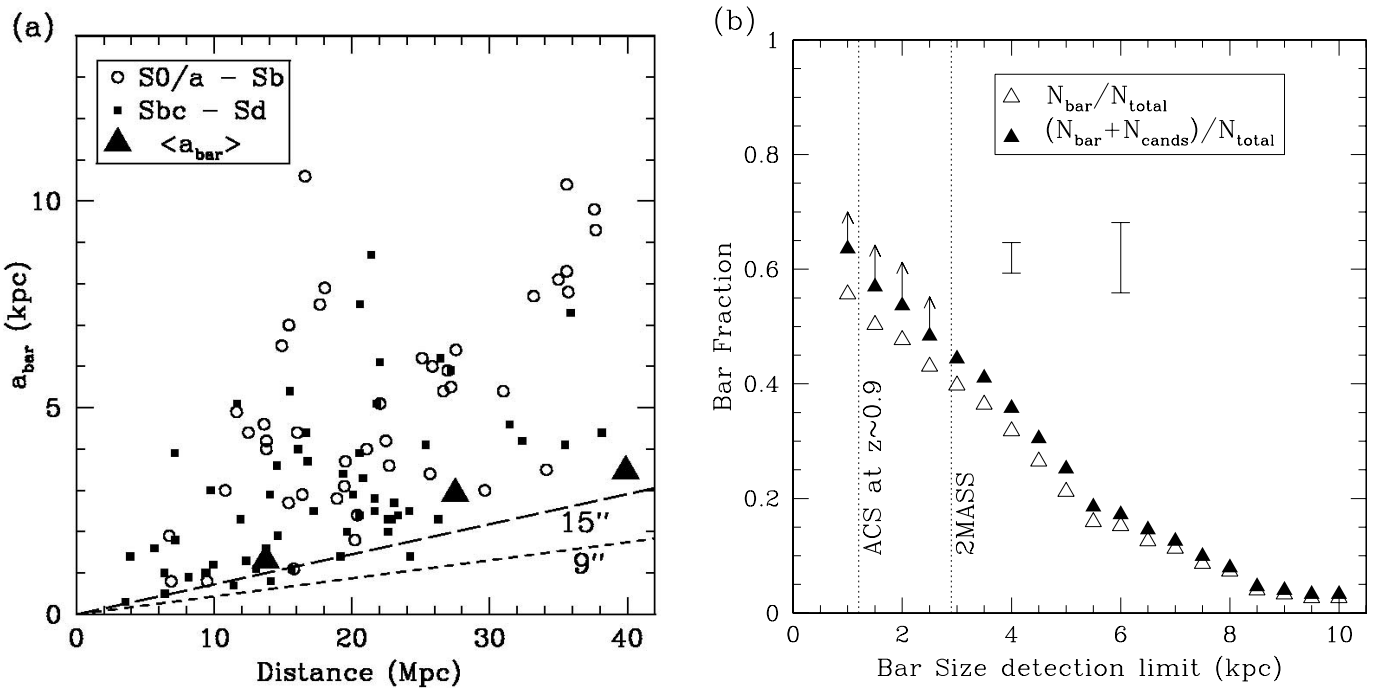

FIG. 6.—(*a*) Projected bar sizes as a function of distance for our 2MASS barred sample. Points corresponding to early-type spirals and late-type spirals are shown following the same symbol convention as Fig. 1. Sensitivity curves of our bar identification method are shown in dotted and dashed lines, corresponding to 9″ and 15″, respectively. Cumulative median projected bar sizes are shown as large filled triangles. The increase of this median size with distance is parallel to the size sensitivity curve of our bar detection method. (*b*) Local bar fraction according to bar size detection limit. Open triangles represent the bar fraction when we only include bars with both ellipticity and P.A. signatures, while filled triangles represent the bar fraction including spirals that we classified as candidates and confirmed to contain a bar by visual inspection. Using 2MASS, we are able to detect all bars with $a_{bar} > 2.9$ kpc out to 40 Mpc. We show this detection limit as well as the $3 \times$PSF detection limit of ACS as dotted vertical lines. Note that the fraction changes dramatically when bar size detection limit changes. Representative Poisson errors for the bar fraction in the case of bar-size detection limits of 4 and 6 kpc are shown, reflecting a decreasing sample size of barred galaxies with increasing bar size.

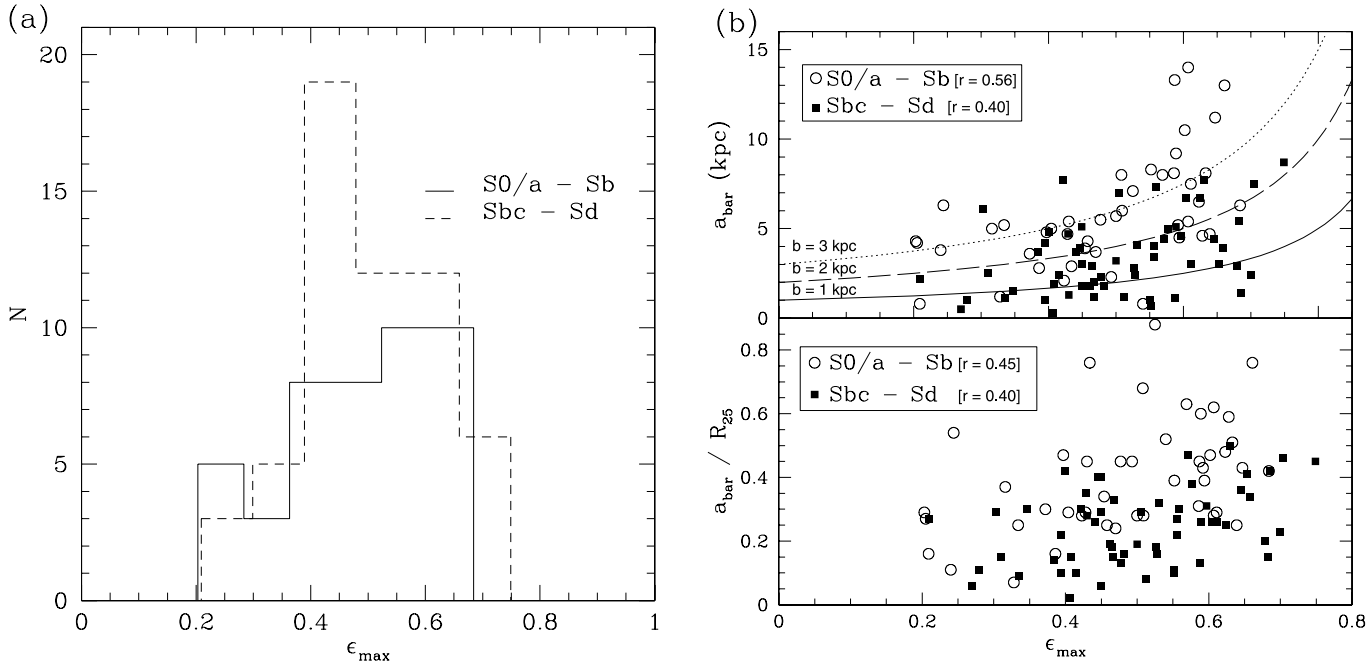

FIG. 7.—(*a*) Distribution of projected ellipticies for 2MASS bars. The distribution for early-type galaxies is shown as a solid line and that of late types, as a dashed line. Both histograms show an increase in number for increasing ellipticity and a sharp decline for bars with $\epsilon \gtrsim 0.75$. Highly elliptical bars correspond to thin, strong bars. (*b*) *Top:* Plot of $a_{\rm bar}$ as a function of projected ellipticity. Symbols for early-type and late-type bars follow the same convention as Fig. 1. We find a weak trend between $a_{\rm bar}$ and $\epsilon_{\rm max}$, which shows that larger bars are stronger; the trend is more evident in the early-type galaxies. Curves of constant semiminor axis values are shown in solid, dashed, and dotted lines for $b = 1$, 2, and 3 kpc, respectively. Note that at a given ellipticity the early-type galaxies lie above the curves. *Bottom:* A similar plot for $a_{\rm bar}/R_{25}$.

be dynamically hotter than a barred spiral. Kinematical studies comparing unbarred and barred galaxies are needed to confirm this hypothesis.

4.2. *Secular Galaxy Evolution*

In the 2MASS sample, early-type barred galaxies tend to host longer bars than late-type galaxies, both in terms of $a_{\rm bar}$ and $a_{\rm bar}/R_{25}$ (see Fig. 5), consistent with previous studies (Elmegreen & Elmegreen 1985; Martin 1995; Laurikainen et al. 2002; Erwin 2005). Martin (1995) reports that early-type bars are on average 3 times larger than late types, slightly higher than our difference of a factor of 2. The sample of Martin (1995) has very few early-type galaxies, whereas our barred sample has more galaxies and a relatively well-balanced distribution of early (44%) and late-type spirals (56%). Early-type spirals are on average more massive than late types and therefore may form longer bars via the bar instability. We also find that bars in early-type galaxies have a larger scatter in sizes than those in late types.

Recent work by Sheth et al. (2005) has shown that a late-type galaxy *cannot* build an early-type bulge solely through gas inflow along a bar; additional processes, such as mergers, are needed to enable the transition of a late-type barred galaxy to an early type. One such scenario of recurrent bar formation has been proposed by Bournaud & Combes (2002). In their simulations, the second-generation bars are shorter than their predecessors. This may be one explanation for the presence of short bars in the early-type galaxies in our 2MASS sample (see Fig. 5).

The distribution of bar ellipticities shows a steep decline in bars with high ellipticites ($\epsilon > 0.6$) and a dearth of bars with $\epsilon > 0.75$ (see Fig. 7*a*). It is possible that these strong bars have been destroyed. Simulations show that bars may dissolve if a sufficiently high concentration of mass accretes at the very centers of the disks (e.g., Norman et al. 1996; Shen & Sellwood 2004). The mass increase is likely driven by the bar-induced gas flow (Kormendy 1982; Friedli & Pfenninger 1991; Friedli & Benz 1993; Regan et al. 1999). Since stronger bars are more efficient in driving gas inward, the central concentration in these strongly barred galaxies may increase rapidly, and may accelerate the process of bar destruction. The decline in strong bars in Figure 7*a* may thus be an indication that stronger bars have evolved more rapidly out of their barred state than weaker barred spirals, and that the strongest bars have already been destroyed.

It is also possible that the drop in the high end of the ellipticity distribution reflects a natural limit on how thin a bar may become either due to the presence of a bulge that limits the size of the bar semiminor axis, or a limit imposed by the stability of the stellar orbits that sustain the bar. The first possibility naturally leads to a bias of more thinner bars in late-type galaxies where bulges are smaller than in earlier type galaxies. However, the ellipticity distribution we find is even more pronounced in the late types (see Fig. 7*a*). Therefore we can rule out the "bulge hypothesis." The other possibility was addressed by Athanassoula et al. (1983) who showed how thin bars have more chaotic orbits. This may also explain the lack of thin bars beyond a certain ellipticity at which a bar becomes unable to sustain itself.

4.3. *Bar Properties*

We find a weak correlation between the bar size and the bar ellipticities (see Fig. 7*b*) with longer bars having somewhat greater ellipticities. This trend is likely to be stronger because the measured ellipticities are underestimated for big-bulged galaxies with thin bars, e.g., bars whose semiminor axis is smaller than the bulge radius. This is because the ellipse fitting routine does not decompose the bulge and disk, and cannot measure an ellipticity with a semiminor axis smaller than the bulge radius. Therefore, the true ellipticity of the thinner early-type spirals is likely to be even higher;

this strengthens the correlation shown in Figure 7*b*. The expected correlation between ellipticity and the semimajor axis for a constant semiminor axis is shown by the curves in Figure 7*b*. The measured ellipticities for early-type spirals are consistently above these curves. This indicates that the bar semimajor axis ($a_{\rm bar}$) changes more rapidly with $\epsilon_{\rm bar}$ than the semiminor axis ($b_{\rm bar}$).

4.4. *The Change in Bar Fraction as a Function of Bar Size*

In deriving a bar fraction it is critical to define the bar population that is being studied. At a fixed angular resolution, the most important selection effect is the decreasing ability to detect smaller bars with increasing distance. This is a serious problem for high-redshift studies aimed at measuring the evolution of the bar fraction, as shown in Figure 3 of Sheth et al. (2003). With our 2MASS sample we can estimate how the bar fraction must change with changing spatial resolutions. In Figure 6*b* we show the cumulative bar fraction for different detection limits of the bar size. The fraction of barred spirals drops from 67% over the entire sample to 36% when we only count bars larger than 4 kpc, and a mere 8% for bars larger than 8 kpc. An important caveat to be noted is that even with our large NIR data set, we are incomplete for the smallest bars. Our bar size detection limit changes from 0.5 to 3 kpc over the volume surveyed ($D \lesssim 40$ Mpc); hence we are only complete for bars with $a_{\rm bar} \gtrsim 3$ kpc. However, this is more than adequate for comparison to high-redshift observations which typically have a similar spatial resolution.

The 2MASS sample thus offers a detailed local comparison sample for the high-redshift studies. As noted in the previous section, the effect of band shifting from the *K* band to the *B* band is likely to be minimal and thus 2MASS is a local anchor for the studies of galaxy evolution in the rest-frame optical.

4.5. *The Local Bar Fraction as an Anchor for High-Redshift Studies*

Our NIR results show that there is not a significant population of veiled barred spirals in the optical, as we discussed in § 4.1. In other words, the *Hubble Space Telescope I*- and *z*-band data now available for high-redshift studies can be used to trace the bar fraction to at least a redshift of $\sim$0.7–0.8 where the observed *I*-band data images galaxies in the rest-frame *B* band. We strongly caution against interpretation of bar fractions for redshifts higher than $z \sim 0.8$ because there is strong evidence that bars completely disappear in the ultraviolet (UV); an example is shown in Figure 1 of Sheth et al. (2003). Other examples are evident in the *GALEX* (*Galaxy Evolution Explorer*) images, which show no bars in nearby galaxies (A. Gil de Paz 2005, private communication).[6] Since UV light is dominated by young ($\lesssim 10^8$ yr) star-forming regions, it may not trace the gravitational potential and bar signatures are likely to be absent in the UV. Any measurement of the bar fraction at $z > 0.8$ in the rest-frame UV is therefore likely to suffer from an abrupt decline in the number of bars as they disappear shortward of the Balmer break. In addition, at $z > 0.8$, observations are affected by coarse linear resolution (see Fig. 3 in Sheth et al. 2003) and the steep decline in the cosmological dimming of the surface brightness. We note that this study, however, is a good analog for high-redshift studies because the angular resolution and shallow depth of 2MASS are similar to the limitations of high-redshift data described above.

Various authors have studied the evolution of the bar fraction with redshift. Sheth et al. (2003) first challenged the previous findings that barred spirals were completely absent at high redshifts (Abraham et al. 1999; van den Bergh et al. 1996, 2000, 2001). Sheth et al. (2003) studied all galaxies in the Hubble Deep Field–North in the WFPC2 *V*, *I*, and NICMOS *H* bands to investigate whether bars were more apparent at the longer NICMOS wavelengths. At $z > 0.7$, the coarse NICMOS data are only able to probe the biggest spirals. Here they find 3/31 barred spirals with an average bar semimajor axis of 6.4 kpc. This fraction is comparable to the 2MASS fraction of 15% for bars with $a_{\rm bar} > 6.5$ kpc, but we note that both samples suffer from small number statistics—large bars are rare and require very large search volumes. With these caveats, Sheth et al. (2003) concluded that there was no strong evidence for an absence of long bars at high redshift.

Following Sheth et al. (2003) two studies have examined the fraction of bars with higher resolution optical Advanced Camera for Surveys (ACS) data. Elmegreen et al. (2004) studied 186 galaxies from the Tadpole field out to $z \sim 1.2$ and reported a nearly constant bar fraction of 0.23 out to $z \sim 1.1$. Jogee et al. (2004) analyzed 258 galaxies from the GEMS survey and reported a similar constant bar fraction of 0.30 out to $z \sim 1$. These studies argue that at high redshifts the bar fraction is measured in the rest-frame *B* band and is therefore comparable to the 0.35 value measured for SB galaxies in the RC3. However, they also claim that the fraction is the same at intermediate redshifts. At redshifts of $0.2 \lesssim z \lesssim 0.7$, the ACS angular resolution and data quality are superb and selection effects noted by Elmegreen et al. (2004) and Jogee et al. (2004) (e.g., surface brightness dimming, coarse resolution, poor S/N) ought to be minimal. Moreover, the rest-frame wavelength data for galaxies at intermediate redshifts is longward of the *B* band. Therefore we would have expected these studies to detect both the SB spirals and the SAB spirals. Their bar fraction should have been comparable to our local NIR result. However, for their bar detection threshold of 1.2 kpc, their measured bar fraction is lower than the 2MASS value of 0.58 by almost a factor of 2.

If the bar fraction is indeed a constant out to $z \sim 0.8$, as suggested by Elmegreen et al. (2004) and Jogee et al. (2004), we would expect the fraction of bars at $z \sim 0.7$–0.8, to be the same as the local (SB+SAB) RC3 fraction measured by eye. One possibility for this discrepancy is the small sample sizes of these existing studies. All of them have less than 300 galaxies over the entire redshift range with which they have attempted to constrain the evolution of the bar fraction. Another possibility is that the bars and galaxies are evolving. For example, if galaxies at $z \sim 1$ are smaller than local galaxies as suggested by Elmegreen et al. (2005) then the bars at these redshifts may also be smaller, and may be undetected by these studies. However, the difference between the local bar fraction and the fraction measured at these higher redshifts may also indicate a potential evolution of the bar fraction with redshift. In order to explore this possibility, we are analyzing the 2 deg^2 COSMOS field to study in detail the evolution of bar fraction to $z \sim 0.8$. The COSMOS data are extremely deep (only half a magnitude shallower than GOODS *z*-band data), and have over 4000 L^* galaxies at $z < 0.8$. With this large and deep data set we will quantify the evolution of the bar fraction and bar sizes while using the results presented here as a local anchor and guide for understanding galaxy evolution.

5. CONCLUSIONS

We have performed a detailed study of 151 2MASS spirals out to 40 Mpc using an ellipse-fitting technique to derive the local fraction of barred spirals and to characterize their properties. We discussed in detail the advantages and shortcomings of our technique for its use as a practical approach in analyzing large data sets for which visual inspection of individual images becomes rapidly inefficient. We discussed how our detailed analysis of the local bar

[6] We have looked at publicly available *GALEX* images of a subset of the 2MASS spiral sample and have found no indication of bars.

population sets the groundwork for studies of galaxy evolution at higher redshifts.

Our main results are the following:

1. We have found a lower limit to the NIR fraction of barred galaxies of 0.59 in the local universe. By complementing our automated bar detection method with visual inspection, the total bar fraction increases to 0.67. This suggests that the bar fraction in the NIR is not significantly different than the bar fraction of 0.63 (SB+SAB) in the optical. This is a promising result for work on the available, expansive data sets of high-redshift galaxies that probe rest-frame optical wavelengths.

2. The typical 2MASS bar extends out to $a_{\rm bar}/R_{25} \sim 0.3$ in radius relative to the underlying blue disk.

3. 2MASS bars have a median semimajor axis of 4.2 kpc. The 2MASS coarse angular resolution and shallow depth favors the detection of larger bars.

4. A weak trend relating bar strength and size appears to be present. The correlation between the bar ellipticity, $\epsilon_{\rm max}$, and $a_{\rm bar}/R_{25}$ is stronger ($r = 0.46$) for early-type galaxies and shows that $a_{\rm bar}$ (and $a_{\rm bar}/R_{25}$) evolves more rapidly with increasing ellipticity than the bar semiminor axis, $b_{\rm bar}$, whose size is regulated by the bulge radius.

5. We find that the mean $a_{\rm bar}/R_{25}$ in early-type spirals is two times larger than in late types, confirming that bars in early-type galaxies are larger than in late types.

6. We show how the measured bar fraction depends critically on the population of bar sizes that can be probed by the observations and detection method. Whereas the bar fraction is 0.64 for bars longer than $a_{\rm bar} = 1$ kpc, the fraction decreases to 0.44 for $a_{\rm bar} > 3$ kpc. Careful consideration of this bar detection threshold must be taken into account for high-redshift studies of the bar fraction.

7. Even after taking into account the ability to resolve bars, the locally measured bar fraction is higher by nearly a factor of 2 than the bar fraction at $z \sim 1$ reported by recent optical ACS studies. Our results do not support the conclusion in these studies that the bar fraction remains constant out to $z \sim 1$. The difference in the bar fraction with these high-redshift studies may be due to small number statistics of the these studies (all have <300 galaxies from $0 < z < 1$). It may, however, indicate a potential evolution of the bar fraction with redshift. We are investigating the evolution of the bar fraction with over four thousand L^* spirals from the COSMOS data set.

We thank our anonymous referee for useful comments that have greatly improved this paper. We are grateful to Michael Regan and Peter Teuben for our discussions on the analysis of this study. We thank Bruce Elmegreen, Linda Sparke, Ron Buta, Leslie Hunt, Peter Erwin, Shardha Jogee, Paul Martini and Luis Ho for their helpful insights. We would also like thank David Block for organizing an excellent conference, "Penetrating Bars Through Masks of Cosmic Dust," and for his hospitality.

This publication makes use of data products from the Two Micron All Sky Survey, which is a joint project of the University of Massachusetts and the Infrared Processing and Analysis Center/California Institute of Technology, funded by the National Aeronautics and Space Administration and the National Science Foundation.

REFERENCES

Abraham, R. G., Merrifield, M. R., Ellis, R. S., Tanvir, N. R., & Brinchmann, J. 1999, MNRAS, 308, 569
Abraham, R. G., Tanvir, N. R., Santiago, B. X., Ellis, R. S., Glazebrook, K., & van den Bergh, S. 1996, MNRAS, 279, L47
Athanassoula, E. 1992a, MNRAS, 259, 328
———. 1992b, MNRAS, 259, 345
Athanassoula, E., Bienaymé, O., Martinet, L., & Pfenniger, D. 1983, A&A, 127, 349
Athanassoula, E., Lambert, J. C., & Dehnen, W. 2005, MNRAS, 363, 496
Barazza, F. D., Jogee, S., & Marinova, I. 2007, in Proc. IAU Symp. 235, Galaxy Evolution across The Hubble Time, ed. F. Combes & J. Palous, in press (astro-ph/0610561)
Block, D., Buta, R., Knapen, J. H., Elmegreen, B. G., Elmegreen, D. M., & Puerari, I. 2004, AJ, 128, 183
Bournaud, F., & Combes, F. 2002, A&A, 392, 83
Buta, R., & Block, D. L. 2001, ApJ, 550, 243
Combes, F., & Gerin, M. 1985, A&A, 150, 327
Das, M., Teuben, P. J., Vogel, S. N., Regan, M. W., Sheth, K., Harris, A. I., & Jeffreys, W. H. 2003, ApJ, 582, 190
de Vaucouleurs, G. 1963, ApJS, 8, 31
de Vaucouleurs, G., de Vaucouleurs, A., Corwin, H. G., Jr., Buta, R. J., Paturel, G., & Fouqué, P. 1991, Third Reference Catalogue of Bright Galaxies, (New York: Springer)
Dickinson, M., Giavalisco, M., & The GOODS Team. 2003, in Proc. ESO/USM Workshop on The Mass of Galaxies at Low and High Redshift, ed. R. Bender & A. Renzini (Berlin: Springer), 324
Elmegreen, B. G., & Elmegreen, D. M. 1985, ApJ, 288, 438
Elmegreen, B. G., Elmegreen, D. M., & Hirst, A. C. 2004, ApJ, 612, 191
Elmegreen, D. M., Elmegreen, B. G., Rubin, D. S., & Schaffer, M. A. 2005, ApJ, 631, 85
Erwin, P. 2005, MNRAS, 364, 283
Eskridge, P., et al. 2000, AJ, 119, 536 (E2000)
———. 2002, ApJS, 143, 73
Friedli, D., & Benz, W. 1993, A&A, 268, 65
Friedli, D., & Pfenninger, D. 1991, in IAU Symp. 146, Dynamics of Galaxies and Their Molecular Cloud Distributions, ed. F. Combes & F. Casoli (Dordrecht: Kluwer), 362
Hackwell, J. A., & Schweizer, F. 1983, ApJ, 265, 643
Heraudeau, P., & Simien, F. 1996, A&AS, 118, 111
Ho, L. C., Filippenko, A. V., & Sargent, W. L. W. 1997a, ApJS, 112, 315
———. 1997b, ApJ, 487, 591
Jarrett, T. H., Chester, T., Cutri, R., Schneider, S. E., & Huchra, J. P. 2003, AJ, 125, 525
Jedrzejewski, R. I. 1987, MNRAS, 226, 747
Jogee, S., et al. 2004, ApJ, 615, L105
Knapen, J., Shlosman, I., & Peletier, R. 2000, ApJ, 529, 93
Kormendy, J. 1979, ApJ, 227, 714
———. 1982, ApJ, 257, 75
Kormendy, J., & Kennicutt, R. C. 2004, ARA&A, 42, 603
Laine, S., Shlosman, I., Knapen, J. H., & Peletier, R. F. 2002, ApJ, 567, 97
Laurikainen, E., Salo, H., & Buta, R. 2004, ApJ, 607, 103 (LSB04)
Laurikainen, E., Salo, H., & Rautiainen, P. 2002, MNRAS, 331, 880
Marinova, I., & Jogee, S. 2007, ApJ, in press (astro-ph/0608039)
Martin, P. 1995, AJ, 109, 2428
Martin, P., & Roy, J. 1994, ApJ, 424, 599
Mulchaey, J. S., & Regan, M. W. 1997, ApJ, 482, L135
Norman, C. A., Sellwood, J. A., & Hasan, H. 1996, ApJ, 462, 114
Ostriker, J. P., & Peebles, P. J. E. 1973, ApJ, 186, 467
Piner, B. G., Stone, J. M., & Teuben, P. J. 1995, ApJ, 449, 508
Regan, M. W., & Elmegreen, D. M. 1997, AJ, 114, 965
Regan, M. W., Sheth, K., & Vogel, S. N. 1999, ApJ, 526, 97
Regan, M. W., Vogel, S. N., & Teuben, P. J. 1997, ApJ, 482, L143
Rix, H-W., et al. 2004, ApJS, 152, 163
Sakamoto, K., Okumura, S. K., Ishizuki, S., & Scoville, N. Z. 1999b, ApJ, 525, 691
Scoville, N. Z., & COSMOS Team. 2007, ApJ, submitted
Scoville, N. Z., Matthews, K., Carico, D. P., & Sanders, D. B. 1988, ApJ, 327, L61
Seigar, M. S., & James, P. A. 1998, MNRAS, 299, 685
Shen, J., & Sellwood, J. A. 2004, ApJ, 604, 614
Sheth, K., Menéndez-Delmestre, K., Scoville, N., Jarrett, T., Strubbe, L., Regan, M. W., Schinnerer, E., & Block, D. L. 2004, in Penetrating Bars Through Masks of Cosmic Dust, ed. D. L. Block et al. (Dordrecht: Kluwer), 319, 405
Sheth, K., Regan, M. W., Scoville, N. Z., & Strubbe, L. E. 2003, ApJ, 592, L13
Sheth, K., Regan, M. W., Vogel, S. N., & Teuben, P. J. 2000, ApJ, 532, 221

Sheth, K., Vogel, S. N., Regan, M. W., Teuben, P. J., Harris, A. I., & Thornley, M. D. 2002, AJ, 124, 2581
Sheth, K., Vogel, S. N., Regan, M. W., Thornley, M. D., & Teuben, P. J. 2005, ApJ, 632, 217
Shlosman, I., Frank, J., & Begelman, M. C. 1989, Nature, 338, 45
Skrutskie, M. F., et al. 2006, AJ, 131, 1163
Teuben, P. 1995, in ASP Conf. Ser. 77, Astronomical Data Analysis Software and Systems IV, ed. R. A. Shaw, H. E. Payne, & J. J. E. Hayes (San Francisco: ASP), 398
Thronson, H. A., et al. 1989, ApJ, 343, 158
van den Bergh, S., Abraham, R. G., Ellis, R. S., Tanvir, N. R., Santiago, B. X., & Glazebrook, K. G. 1996, AJ, 112, 359
van den Bergh, S., Cohen, J. G., & Crabbe, C. 2001, AJ, 122, 611
van den Bergh, S., Cohen, J. G., Hogg, D. W., & Blandford, R. 2000, AJ, 120, 2190
Whyte, L. F., Abraham, R. G., Merrifield, M. R., Eskridge, P. B., Frogel, J. A., & Pogge, R. W. 2002, MNRAS, 336, 1281 (W2002)
Wozniak, H., & Pierce, M. J. 1991, A&AS, 88, 325
Zheng, X. Z., Hammer, F., Flores, H., Assémat, F., & Rawat, A. 2005, A&A, 435, 507